Support Information

Microstructural Stiffness Engineering of Low Dimensional Metal Halide Perovskites for Efficient X-ray Imaging

Yangmin Tang,[1,2,7] Guiqiang Pu,[3,7] Chengbin Kang,[4] Chenyang Li,[5] Xiaoze Wang,[6] Machao Wang,[1,2] Hui Bi,[1,2] Wei Chen,[5] and Jiacheng Wang[1,3]**

[1] The State Key Laboratory of High Performance Ceramics and Superfine Microstructure, Shanghai Institute of Ceramics, Chinese Academy of Sciences, Shanghai 200050, China

[2] Center of Materials Science and Optoelectronics Engineering, University of Chinese Academy of Sciences, Beijing 100049, China

[3] Zhejiang Key Laboratory for Island Green Energy and New Materials, Institute of Electrochemistry, School of Materials Science and Engineering, Taizhou University, Taizhou 318000, China

[4] Department of Applied Physics, The Hong Kong Polytechnic University, Hung Hom, Kowloon, Hong Kong 999077, China

[5] Department of Materials Design and Innovation, University at Buffalo, The State University of New York, Buffalo, NY 14260, USA

[6] MOE Key Laboratory for Analytical Science of Food Safety and Biology and State Key Laboratory of Photocatalysis on Energy and Environment, College of Chemistry, Fuzhou University, Fuzhou, 350108, China

[7] These authors contributed to this work equally.

Corresponding author: jiacheng.wang@mail.sic.ac.cn (J. W.); wchen226@buffalo.edu (W. C.);

Experimental Section

Materials

Rubidium chloride (99.9%), rubidium bromide (99.9%), silver chloride (>98%), and silver bromide (98%) were purchased from Adamas and used as received.

Material Synthesis

Rb_2AgX_3 were synthesized by a facile solid-state method. Stoichiometric amounts of raw materials, RbX and AgX were weighed and put in a ball-milling machine and ball-milled for 4 h for homogeneous mixing. For Rb_2Ag_3, the ratio between RbCl and AgCl is 2:1. For Rb_2AgCl_2Br, the ratio between RbCl, AgCl, RbBr, AgBr is 4:2:2:1. For Rb_2AgCl_2Br, the ratio between RbCl, AgCl, RbBr, AgBr is 2:1:4:2. For Rb_2AgBr_3, the ratio between RbBr and AgBr is 2:1.

Materials Characterization

X-ray diffractometer (XRD) measurements for Rb_2AgX_3 samples were performed using a Bruker D8 ADVANCE X-ray diffractometer (Cu-Kα radiation, λ = 1.5406 Å). The 2θ range was recorded from 10 to 80° with a scan step size of 0.02°. Scanning electron microscope (SEM) images and EDS elemental mapping analysis were using an FEI Magellan 400 L XHR microscope equipped with an energy dispersive spectrometer. The Raman spectroscopy was performed using a Horiba LabRAM HR Evolution spectrometer with a 532 nm laser excitation wavelength. The JEOL 2100F transmission electron microscope (TEM) was used to investigate the morphology and structure of the powders. X-ray photoelectron spectroscopy (XPS) was used to analyze the chemical environments, utilizing a Thermo Scientific K-Alpha spectrometer and an Al K X-ray beam (1486.6 eV) as the radiation source. The photoluminescence (PL) and photoluminescence excitation (PLE) spectra were collected using Edinburgh Instruments, FLS 980 with a Xenon Arc Lamp as a light source. FLS 980 was also used to obtain the X-ray excited luminescence (XEL) spectra, and the spectrometer was instrumented with an X-ray tube (tungsten target) and operated at 50 kV and 2 mA. Time-resolved photoluminescence (TRPL) spectra were also measured using a

spectrofluorometer (Edinburgh Instruments, FLS 980). All temperature variation measurements were performed with an additional device. The TG data were collected under N_2 atmosphere (PerkinElmer Instruments, Diamond TG/DSC6300). The luminescent photograph was recorded under the excitation of a portable mercury lamp (UV 254 nm). ESR spectra were collected using a Bruker A300 (70 K, 9.8536 GHz).

Device fabrication

The PDMS and scintillator powder were mixed in a 10:1 mass ratio and stirred to form a uniformly mixture gel. The mixture was then evacuated in a vacuum tank to eliminate air bubbles. The mixture was then evenly scraped onto a PET film (10 cm * 10 cm). The mold was heated at 80 °C and hold for 5 hours.

Device characterization

X-ray imaging measurements were carried out using a home-built system consisting of an X-ray source (TUB-00083-AG2, Moxtek Inc.), scintillator film, and a digital camera. The radiation dose of X-rays was controlled by changing the current and voltage of the X-ray source. By adjusting the voltage and current of the X-ray source, the radiation dose can be regulated. The operational voltage and current of the X-ray source range from 0 to 50 kV and 0 to 80 μA, respectively. In the X-ray imaging process, the sample was put between the scintillator screen and the X-ray source. A camera was utilized to capture images from the other side of the scintillator film. To protect the camera from X-ray damage, a reflector was also utilized.

Computational Methods

This study employed Density Functional Theory (DFT) calculations and Crystal Orbital Hamilton Population (COHP) analysis to investigate the electronic structure and bonding characteristics of the system.[1] DFT calculations were performed using the Vienna Ab initio Simulation Package (VASP). The exchange-correlation functional was treated within the Heyd-Scuseria-Ernzerhof (HSE) potential, which is a screened-exchange hybrid functional used to improve the accuracy of the electronic structure

calculations.[2-4] Using the HSE06 functional to perform calculations could ensure accuracy in predicting semiconductor bandgaps. The plane wave energy cutoff of 265 eV was used for all calculations. The Brillouin zone was sampled using a Monkhorst-Pack k-point grid for structural optimization, while a denser grid was used in electronic calculations.[5] Following the Franck-Condon principle, the excited state was treated by Delta Self-Consistent Field (ΔSCF) method. The excited state was simulated by exciting an electron from the valance band edge to the conduction band, leaving a hole in the valence band without introducing a net charge into the system. The excited structures were obtained by optimizing the corresponding structures with one exciton incorporated. The ΔSCF method has been widely employed to study the photoexcited and related structural changes in semiconductors.[6] All structures were fully relaxed until the forces on each atom were less than 0.01 eV/Å. The COHP analysis was performed using the Local Orbital Basis Suite Towards Electronic-Structure Reconstruction (LOBSTER) package. [7, 8] This method allows the decomposition of the total density of states into contributions from individual atomic orbitals, providing detailed insight into the bonding characteristics of the system. This method is particularly useful for analyzing complex systems in which the bonding characteristics are not easily discernible. The COHP curves were integrated up to the Fermi level to obtain the integrated COHP (ICOHP), which serves as a measure of the strength and character (bonding or antibonding) of the interactions.[9] Furthermore, ICOHP can also provide information about the energy distribution of the molecular orbitals and the relative contribution of each atomic orbital to the overall density of states, which is useful for understanding the electronic structure of the system.

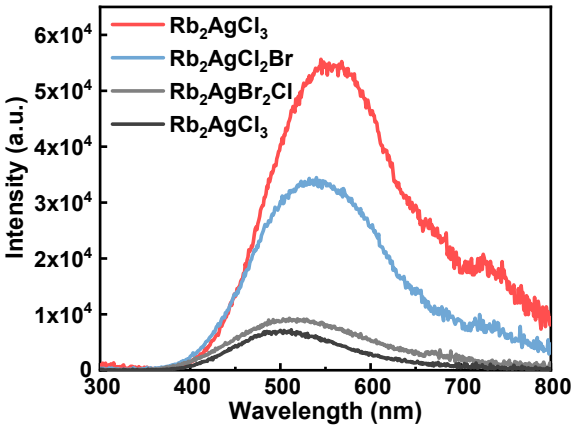

Fig. S1. X-ray excited luminescence spectra of Rb_2AgX_3.

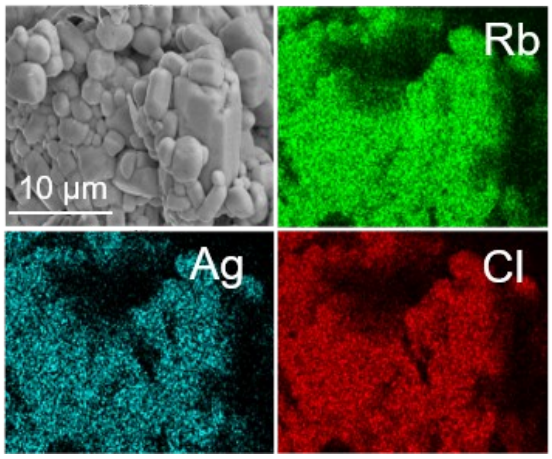

Fig. S2. Scanning electron microscope (SEM) images and element mapping of Rb_2AgCl_3.

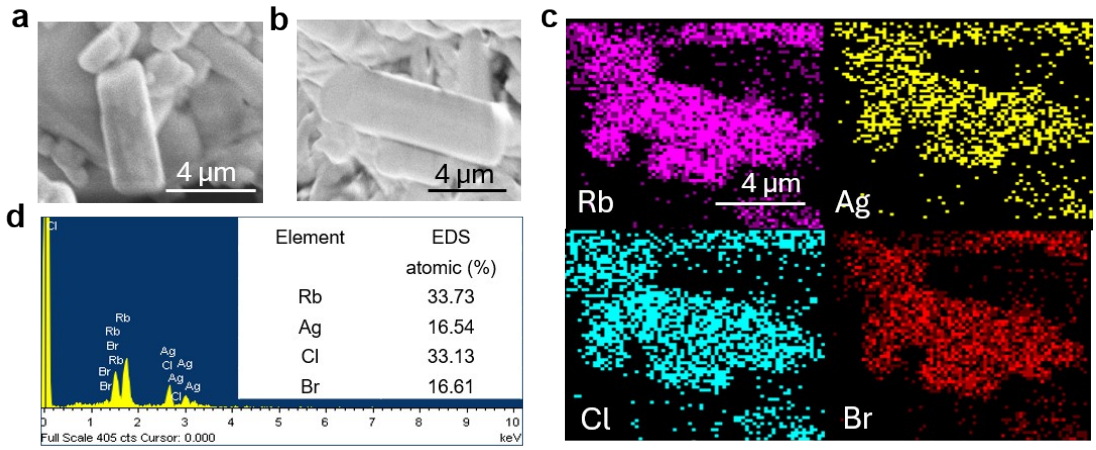

Fig. S3. (a) and (b) SEM images of Rb_2AgCl_2Br. (c) Element mapping images of Rb_2AgCl_2Br, which obtained from (b). (d) Energy dispersive spectroscopy on the SEM (EDS-SEM) of Rb_2AgCl_2Br shows that the atomic ratio of Rb, Ag, Cl, and Br is 2:1:2:1.

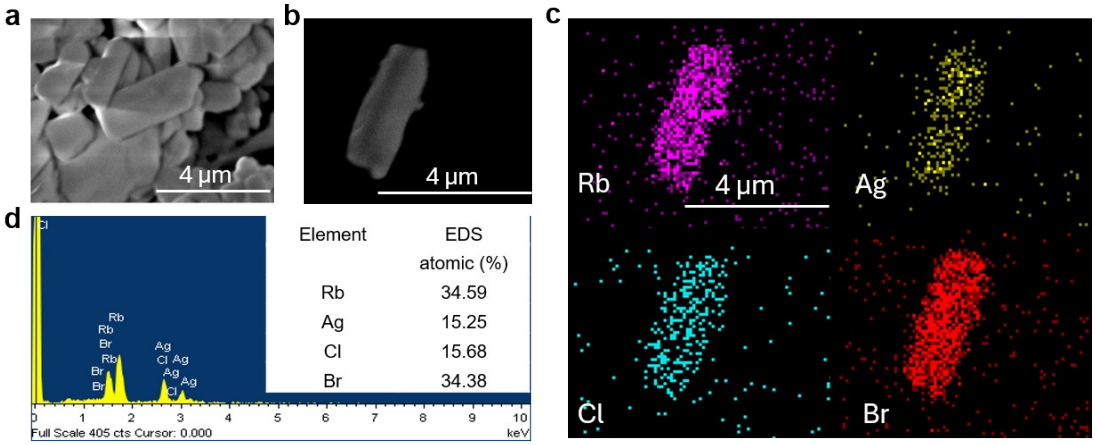

Fig.S4. (a) and (b) SEM images of $Rb_2AgClBr_2$. (c) Element mapping images of $Rb_2AgClBr_2$, which obtained from (b). (d) Energy dispersive spectroscopy on the SEM (EDS-SEM) of $Rb_2AgClBr_2$ shows that the atomic ratio of Rb, Ag, Cl, and Br is 2:1:1:2.

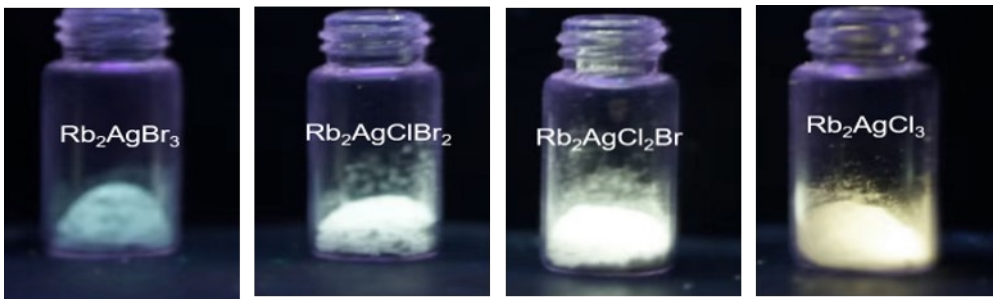

Fig. S5. Photos of Rb_2AgX_3 under 254 nm excitation.

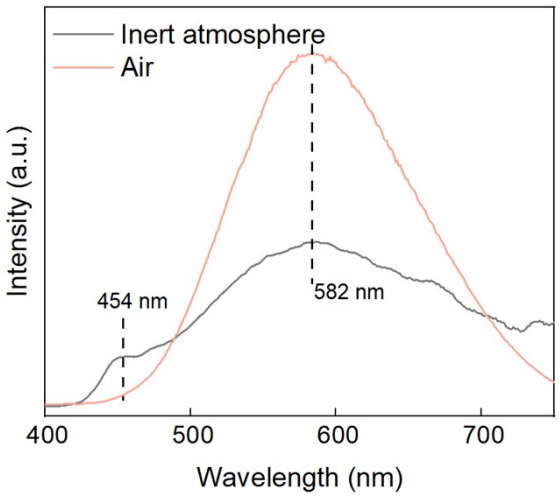

Fig. S6. Photoluminescence spectra of Rb_2AgCl_3 synthesized in inert atmosphere and in air.

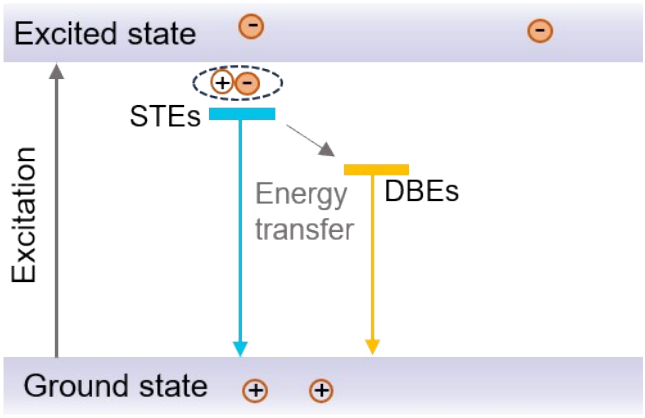

Fig. S7. Schematic diagram of the proposed photophysical mechanism in Rb_2AgCl_3.

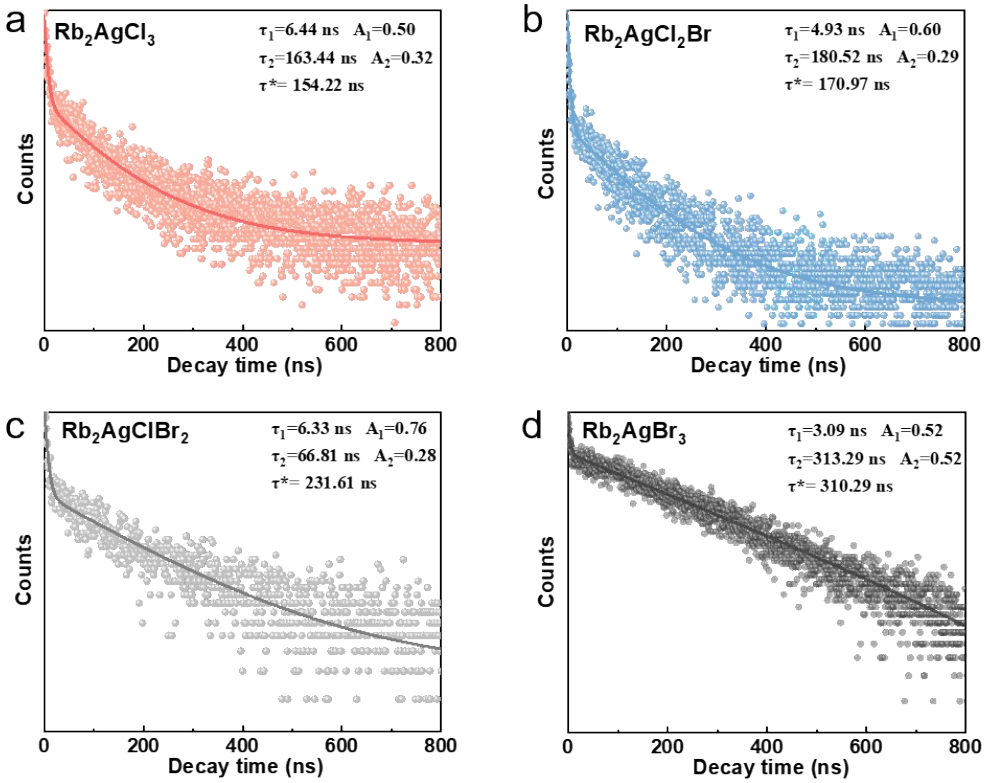

Fig. S8. Time-resolved photoluminescence (TRPL) decay curves of a) Rb_2AgCl_3, b) Rb_2AgCl_2Br, c) $Rb_2AgClBr_2$, and d) Rb_2AgBr_3.

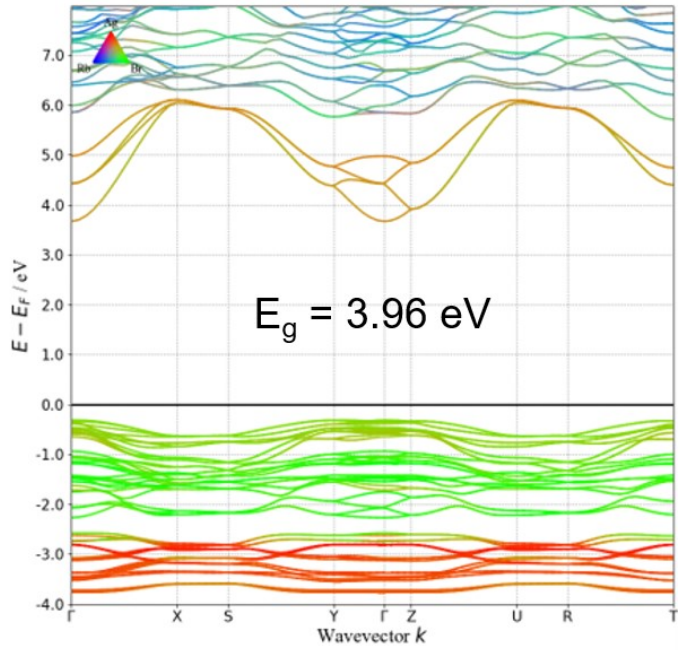

Fig. S9. Band structure of Rb_2AgBr_3.

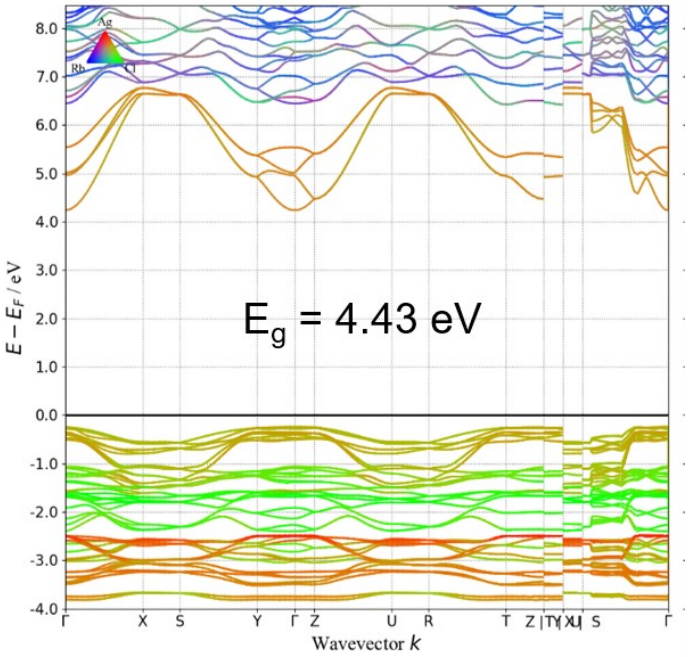

Fig. S10. Band structure of Rb_2AgCl_3.

Table S1. Atomic concentrations obtained from XRS measurements

	Rb (%)	Ag (%)	Cl (%)	Br (%)
Rb_2AgCl_3	36.01	16.87	47.12	
Rb_2AgCl_2Br	39.6	17.6	29.64	13.17

$Rb_2AgClBr_2$	40.76	16.34	16.23	26.67
Rb_2AgBr_3	38.98	18.36	42.66	

Table S2. Calculated lattice parameters of Rb_2AgBr_3 in the ground (uncharged) and excited states (charged).

	uncharged	charged	difference	relative change
a	4.6998	4.6126	-0.0871	1.854%
b	9.7839	9.5628	-0.2211	2.259%
c	19.0295	18.4919	-0.5376	2.825%

Table S3. Calculated lattice parameters of Rb_2AgCl_3 in the ground (uncharged) and excited states (charged).

	uncharged	charged	difference	relative change
a	4.5164	4.4266	-0.0897	1.987%
b	9.3338	9.1303	-0.2035	2.180%
c	18.1190	17.6155	-0.5035	2.779%

References

1. R. Dronskowski and P. E. Bloechl, *J. Phys. Chem.*, 1993, **97**, 8617-8624.
2. G. Kresse and J. Furthmüller, *Comput. Mater. Sci.*, 1996, **6**, 15-50.
3. G. Kresse and J. Furthmüller, *Phys. Rev. B*, 1996, **54**, 11169.
4. A. V. Krukau, O. A. Vydrov, A. F. Izmaylov and G. E. Scuseria, *J. Chem. Phys.*, 2006, **125**.
5. H. J. Monkhorst and J. D. Pack, *Phys. Rev. B*, 1976, **13**, 5188.
6. C. Zhou, H. Lin, H. Shi, Y. Tian, C. Pak, M. Shatruk, Y. Zhou, P. Djurovich, M. H. Du and B. Ma, *Angew. Chem.*, 2018, **130**, 1033-1036.
7. S. Maintz, V. L. Deringer, A. L. Tchougréeff and R. Dronskowski, *Journal*, 2016.
8. R. Nelson, C. Ertural, J. George, V. L. Deringer, G. Hautier and R. Dronskowski, *J. Comput. Chem.*, 2020, **41**, 1931-1940.
9. S. Maintz, V. L. Deringer, A. L. Tchougréeff and R. Dronskowski, *J. Comput. Chem.*, 2013, **34**, 2557-2567.